NJC

Accepted Manuscript

This article can be cited before page numbers have been issued, to do this please use: M. ., A. Singh, P. Raj, R. Kaur, A. Singh, N. Kaur and N. Singh, *New J. Chem.*, 2017, DOI: 10.1039/C6NJ03763A.

ROYAL SOCIETY OF CHEMISTRY

rsc.li/njc

View Article Online
DOI: 10.1039/C6NJ03763A

Journal Name

ARTICLE

Zwitterionic Liquid (ZIL) Coated CuO as an Efficient Catalyst for the Green Syntheses of Bis-Coumarins derivatives *via* One-Pot Multi-component Reactions Using Mechanochemistry

Received 00th January 20xx,
Accepted 00th January 20xx

DOI: 10.1039/x0xx00000x

www.rsc.org/

Mayank,[a] Amanpreet Singh,[a] Pushap Raj,[a] Randeep Kaur,[b] Ajnesh Singh,[c] Navneet Kaur[d] and Narinder Singh*[a]

A convenient solvent free strategy for the synthesis of bis-coumarins has been developed using zwitterionic liquids **(ZILs)** coated copper oxide (CuO) using mechanical ball milling. The zwitterionic liquids are fabricated of imidazolium/benzimidazolium and sulfonate/carboxylate based moieties. The **ZIL** has offered an interesting multifunctional opportunity to immobilize them over CuO through anionic part and the cationic part is freely available for catalytic applications. The hybrid catalysts are fully characterized with scanning electron microscopy (SEM), transmission electron microscopy (TEM), energy-dispersive X-ray (EDX), powder X-ray diffraction (PXRD), cyclic voltammetry (CV), solid state UV-Vis absorption and emission spectroscopic methods. The three zwitterionic liquid based and CuO coupled hybrid catalysts **(ZIL@CuO1-3)** have been generated with diversity in size, shape, photophysical signature and electrochemical properties. The supramolecular assembly of **ZIL** and CuO in **ZIL@CuO1** has extensively enhanced the catalytic activity as compared to their parent components individually as well as other two tested hybrid materials **ZIL@CuO2-3**. Furthermore, the reaction conditions are optimized through varying thenumber of balls, milling time and milling speed. The reaction mechanism has been elucidated using ^{1}H NMR spectroscopy and all the final products have been fully characterized with spectroscopic methods. Finally, the performance of reaction at multi-gram scale is also detailed; high eco-scale score and low E-factor are the most pleasing features of the methodology; thus authenticate its use for eco-friendly synthesis of bis-coumarins and offers the advancements over the existing literature.

Introduction

Heterocyclic compounds are the backbone of the medicinal chemistry possessing therapeutic efficacy varying from simpler COX inhibitors to complex signaling cascades.[1-4] On the other hand, the heterocyclic compounds are the integral part of biological system such as genetic material, energy sources, structural as well as enzymatic proteins.[5] Thus, to understand the bio-chemical processes and development of new chemical entities (NCEs) synthetic strategies are reported and nevertheless, there is room for the improvement to cater the need of sustainable development.[6, 7] In general, the new synthetic strategy must sculpture the complex molecular structure from the easily accessible commercial building blocks.[7] However, majority of reported methods involves the extensive use of organic solvents and tedious post reaction workup which restrict its industrial scale up-gradation.[8, 9] Moreover the drawbacks including low yield, catalyst reuse inability and thus improved method for the synthesis of heterocyclic compounds such as coumarin derivatives is of high demand because this category of compounds have pronounced pharmacological activities including anti-inflammatory,[10] antimicrobial,[11] antiviral,[12]anti-coagulant,[13] and anti-cancer [13]; which warrant these as attractive moiety in drug designing.[13] Within the context of improved methods for coumarin derivatives; the green synthetic approach is the significant progression toward the sustainable development of pharmaceutical industry and hence some serious efforts have been made in this direction.[14] The ball milling is smart green synthetic methodology, which involves solvent free synthesis of organic molecules and even prominent for one pot multicomponent reactions including oxidations, reductions, condensations, Wittig reactions, asymmetric Michael addition reactions, Baylis–Hillman reactions, 1-3,dipolar cycloaddition, enamine formation, transition metal-catalyzed coupling reactions and synthesis of pyrimidines and variety of heterocycles.[15-20]Furthermore, many metal catalysts have been fabricated and successfully used for the synthesis of multiple compounds such as pyrimidine derivatives,[21] C-C bond formation,[22] amino andhydroxyl substituted dehydrophenylalanine derivatives,[23]benzothiazole, benzimidazole andbenxoxazole derivatives.[16]The synthesis of bis-coumarins using ball milling with efficient catalyst having high eco-scale score (Table ST1, supplementary information)[16] and low E-factor (Table ST2)[16] is relatively unexplored research arena. Under present investigation, we have made attempts to improve the shortcomings of existing methodologies in terms of green solvent; energy source and catalyst reuse ability(Table ST3). To achieve the desired objective, we have engineered supramolecular catalysts,

[a] Department of Chemistry, Indian Institute TechnologyRopar, Punjab 140001, India. E-mai: nsingh@iitrpr.ac.in
[b] Department of Chemistry, Guru Nanak Dev University Amritsar, Punjab 143001, India
[c] Department of Applied Sciences and Humanities, Jawaharlal Nehru Government Engineering College, Sundernagar, Mandi (H.P.) 175018, India.
[d] Department of Chemistry, Punjab University, Chandigarh,160014 India.

View Article Online
DOI: 10.1039/C6NJ03763A

which are fabricated of zwitterionic liquids **(ZILs)**(Figure 1) coated copper oxide (CuO).

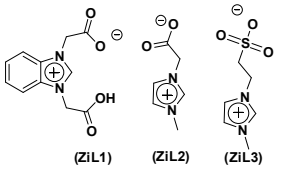

Figure 1. Chemical structures of zwitterionic liquids **ZIL 1-3**.

The motivation for the use of hybrid assembly of **ZIL@CuO** is due to the distinctive implementation of such type of ILs in heterocyclic synthesis, Biginelli reaction,[24] alkylation reaction,[25] Diels-Alder reaction[26] and Michael addition reaction[27] and multicomponent reactions. Furthermore, excellent organic transformations were introduced using ILs/ZILs-metal hybrid system showing its importance in organic synthesis. [16, 28-30]In this context, CuO was also investigated as versatile catalyst for multiple organic transformations.[31, 32] We envisioned the hybrid assembly of **ZIL@CuO** as efficient and reusable catalyst fulfilling special requirements in solvent free synthesis. The cationic part of **ZIL** is composed of imidazolium/benzimidazolium; while the sulfonate/carboxylate are the anionic moieties. The **ZILs** are designed in such a way that they must present multifunctional prospects such as anionic part immobilize them over CuO and the cationic part obligate the synergistic catalysis in augmentation to CuO. Herein, solvent free synthesis tends to reduce wastage of organic solvents as in solvent mediated synthesis (ST 3) resulted to penalty pointsin green chemistry metrics of the reaction.

Results and Discussion

ZIL coating and structurally diverse ZIL@CuO formation:ZILs are the special class of ionic liquids (ILs), which are composed of cationic part prevailed in ionic liquids.[33] The choice of such types of **ZILs** is based upon the splendid activities of **ILs** as catalysts in organic synthesis mostly due to precise control over Bronstead/Lewis acidity that is mandatory for widespread catalytic activities.[25] Moreover, the ILs are the foremost choice of synthetic chemists due to their least vapor pressure, ability to solubilize wide range of compounds, reusability and recyclability associated with them. [34, 35] In order to customize the catalytic activities required for the eco-friendly synthesis of bis-coumarins; the **ZIL1-3** were planned with diversity in the cationic and anionic part and were synthesized using reported methods.[36, 37] The **ZIL1-3** were characterized with NMR Spectroscopy, elemental analysis and the zwitterionic structure of **ZIL1** was illustrated with the single crystal structure (Figure 2).

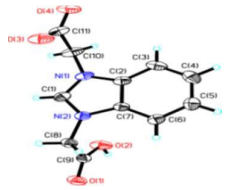

Figure 2.ORTEP diagram along with atom numbering scheme of complex **ZIL1** with 40% probability thermal ellipsoids

Singe crystal X-ray structure determination revealed that compound **ZIL1** crystallizes in triclinic crystal system and consists of two molecules of compound **ZIL1**. Two oxygen atoms O4 and O5 of carboxylic groups are disordered over two positions each. One of the carboxylic group present on **ZIL1** is unionized while other is ionized which is counter balancing the positive charge of imidazolium nitrogen atom. The ORTEP diagram along with atom numbering scheme of complex is shown in Figure 2. The selected bond lengths and bond angles are given in Table ST4. In the crystal lattice, different moieties are interacting with each other through O-H…O hydrogen bonding which result in formation of chains of **ZIL1** moieties. These chains are held together in crystal lattice through number of C-H…O hydrogen bonds and π–π stacking interactions whereas distance between centroids of two phenyl rings is 3.666Å, while the closest C…C distance is C6…C18= 3.355 Å. The packing diagram of compound **ZIL1** is shown in Figure SF1 (Supplimentary information). The hydrogen bonding parameters are given in Table ST5.

Our mandate is to perform the solvent free synthesis using ball mill; and metal oxides have been used to comply the catalysis in ball mill.[38] Hence, to realize the synergistic catalytic effect of **ZIL** and metal oxide; we have used the **ZILs** as structure directing agents as well as catalytic module with CuO. In general, structure directing agents immobilize themselves on the surface of the metal oxide and determine the size, shape and morphology of the final catalyst. The hybrid catalysts **ZIL@CuO** were prepared using sol-gel method.[38, 39] Copper nitrate was dissolved in 100 ml of double distilled water to form 0.1 M solution. The **ZILs** were than incorporated to the aforementioned solution. The resulting solution was stirred vigorously for fifteen minutes. Finally, 0.1 M solution of NaOH was added dropwise to the vigorously stirred solution. Refluxing for 2 h was performed to get **ZIL@CuO1-3**. Similarly, bare CuO nanoparticles without **ZIL** were also produced and precisely controlled identical conditions were applied in all cases. The as-prepared **ZIL@CuO1-3** were characterized with SEM, TEM, powder XRD and their size distribution was realized with DLS based particle size analyzer (Figure 3). The SEM analysis of **ZIL@CuO1** (Figure 3, A)has shown the formation of flakes, which is expected due to the bidentate nature of **ZIL1**. Thus, it is expected that two carboxylate group of each **ZIL1** are not coordinating with same CuO particle rather they are diverging to coordinate with different CuO and hence endorsing the formation of sheet. Moreover, the flakes are arranged in a particular pattern, presumably due to the π- π stacking prevailed in the benzimidazolium moieties as clearly noticed in the crystal structure of **ZIL1**. Unlike **ZIL1**, the **ZIL2-3** are the unidentate ligands; thus, they are not anticipated to yield any supramolecular assembly and as per expectation, TEM images of **ZIL@CuO1-3** further clarified the fact. In case of **ZIL@CuO1** (B) supramolecular assembly production was anticipated by the TEM images**.** TEM images of **ZIL@CuO2-3** (C and D respectively) showed the formation of spherical particles. Furthermore, PXRD studies were performed for CuO as well as **ZIL@CuO1-3**. The PXRD pattern of CuO (E) clarified the single phase CuO nanoparticles formation.

View Article Online
DOI: 10.1039/C6NJ03763A

The diffraction data was found to be in good agreement with the JCPDS card of CuO (JCPDS 80- 1268). Average crystallite size (L) was calculated using Scherrer's equation "$L = 0.9\lambda/\beta\cos\theta$" where λ is the X-ray wavelength (1.5405 Å), and β is full width at half maximum in radian. The Crystallite size calculated for bare CuO and **ZIL@CuO1-3** was found to be 25, 8, 17 and 21 nm respectively. The, significant change in PXRD pattern compared to CuO, was observed for **ZIL@CuO1-3** and crystallinity was thus extensively changed upon **ZIL** coating. Major variation was observed for **ZIL@CuO1**; while for **ZIL@CuO2-3** are expected to produce similar size. DLS histograms were also recorded to quantify the average size and size distributions of catalysts produced. The average size of **ZIL@CuO1**(F), **ZIL@CuO2** (G) and **ZIL@CuO3** (H) were found to be 447 nm, 100 nm and 85 nm respectively. Thus, size distribution for **ZIL@CuO1** was significantly higher compared to **ZIL@CuO2&3**. The EDX data was recorded to confirm the presence of organic part along with CuO. In case of **ZIL@CuO1** along with base element copper and oxygen, carbon as well as nitrogen was also observed (I). Similarly carbon and nitrogen for **ZIL@CuO2** (J) and carbon, nitrogen and sulfur for **ZIL@CuO3** (K)along with copper and oxygen were confirmed through EDX data. The abovementioned results are in well agreement with elements profile of **ZIL1-3** and provided evidences for the presence of proper **ZIL** coating on the surface of CuO nanoparticles for **ZIL@CuO1-3**.

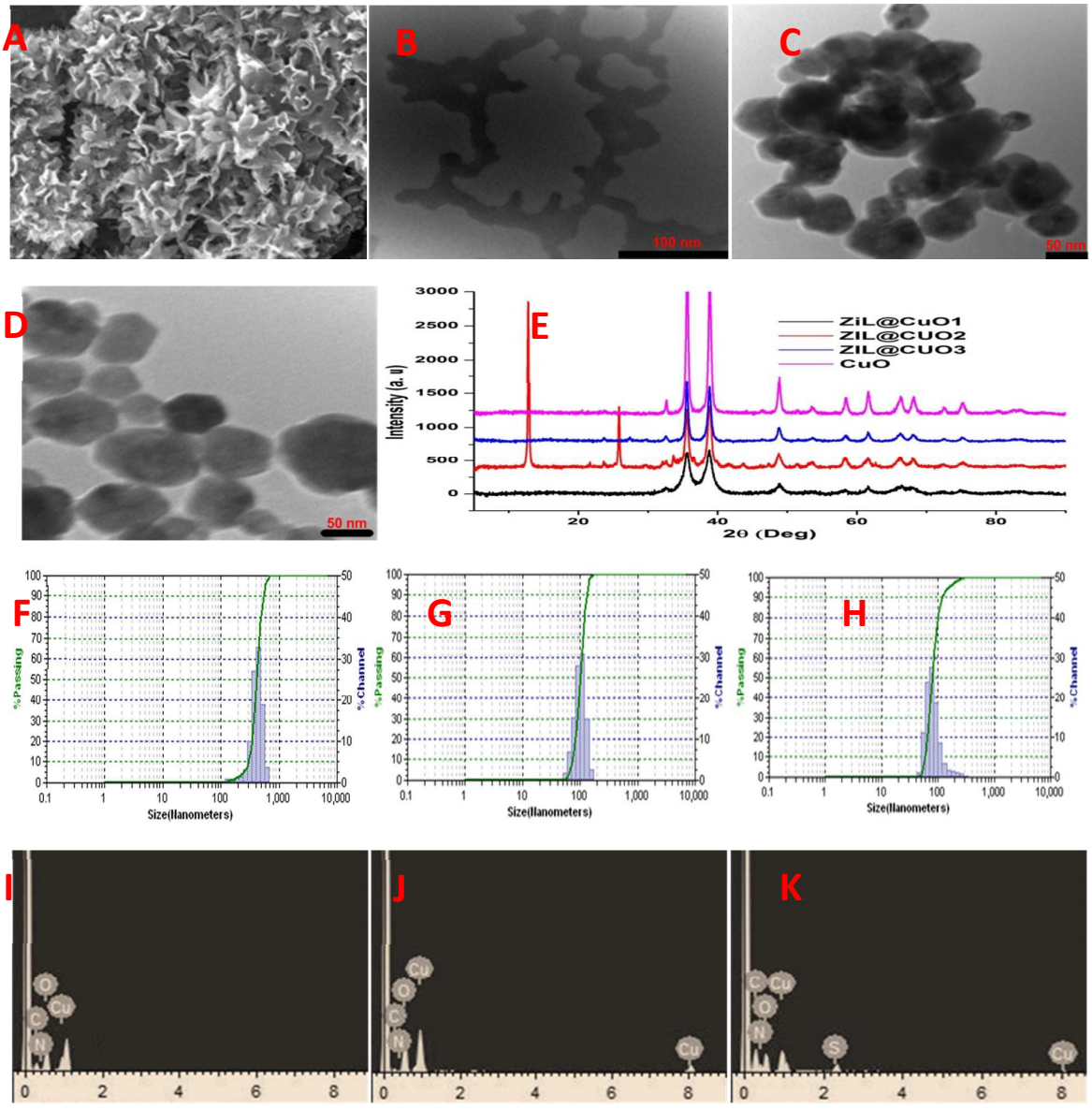

Figure 3. (A), SEM images of **ZIL@CuO1**; **(B-D)**, TEM images of **ZIL@CuO1-3;(E)**, PXRD of **ZIL@CuO1-3; (F-H),**DLS of **ZIL@CuO1-3 and (I-K)**, **EDX of ZIL@CuO1-3**respectively.

View Article Online
DOI: 10.1039/C6NJ03763A

Journal Name

ARTICLE

Photophysical properties of ZIL@CuO: The Lewis acid directed catalyst may govern through the photophysical signature of the catalyst and thus possibly these properties may decide the fate of reactivity. In this intension, the photophysical properties are evaluated by recording the UV-Vis absorption and emission spectra of **ZIL@CuO1-3** (Figure 4, A&B respectively);further the results are compared with the pure CuO.When **ZILs** were used as surface directing agent in the synthesis of **ZIL@CuO1-3** through sol-gel method, the absorption spectrum should depicted changes compared to CuO, happening in the system during nucleation and crystal growth of **ZIL@CuO1-3.** The solid state absorption spectrums of precipitated **ZIL@CuO1-3** were recorded and results were compared with solid state absorption spectrum of bare CuO. The spectrum of bare CuO revealed clearer and broad band which became diminished with **ZIL@CuO1-3**. Further, blue shift in case of **ZIL@CuO1-3** with respect to bare CuO was also observed. Based on the absorption profile, by implementing tauh plot, band gap for CuO and **ZIL@CuO1-3** was established. Band gap for CuO was found to be 1.3 eV, which was exactly as documented in literature.[40] For **ZIL@CuO1-3** the band gap was comparatively higher and found to be 1.7, 2.1 and 1.9 eV respectively. With the availability of capping agents as in case of **ZIL@CuO1-3**, size of produced nanoparticles tends to reduce compared to bare CuO. Here, size dependency of band gap in case of nanoparticles was found to be inversely allied and is correlating with already documented results.[41] To understand the emission profile of materials at room temperature the fluorescence spectra of **ZIL@CuO1-3** have been surveyed with excitation at 330 nm. The CuO has exhibited the emission at 402 nm and this is described as band edge emission of CuO.[42] However, the **ZIL@CuO1-3** have pronounced broad band and it is plausible to deconvulate this band into different emission states on account of defect-related emission or surface impurities including intrinsic defects, interstitial metal ions, and oxygen vacancies survived during crystal growth of CuO.[43]

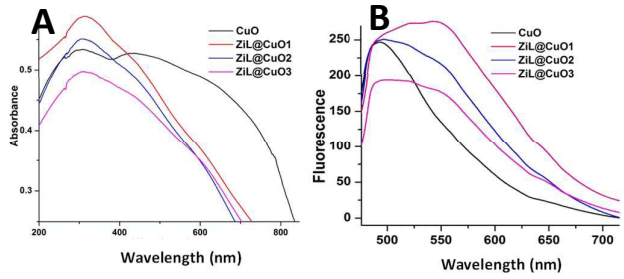

Figure 4. (A) Solid state UV-Vis absorption spectra of CuO and **ZIL@CuO1-3** (B) Solid state emission profile of **ZIL@CuO1-3**.

ZIL coating tends to change theelectrochemical behaviour in case of ZIL@CuO1-3: The electrochemical behaviour of **ZIL@CuO1-3** were studies through cyclicvoltammetry in aqueous medium containing 0.1 M tetrabutyl ammonium perchlorate as a supporting electrolyte using Ag/AgCl and Pt based electrodes. The parameters used include 1500 mV as initial as well as final potential and -1500 mV as switching potential. The redox behavior of **ZIL@CuO1** showed cathodic peak at - 0.549 mV corresponding to Cu^{2+} /Cu and anodic peak occur at - 0.344 mV attributed to Cu/Cu^{2+}.[44] The redox process of **ZIL@CuO1** are quassi-revesible in nature which was confirmed through scan rate experiment. It was observed from the scan rate experiment that the δE value is greater than 59/n mV and increase with increase in the scan rate. The ratio of cathodic peak current to anodic peak current is also morethanone ($I_c/I_a>1$). These result confirmed the quassi-revesible redox behaviour of **ZIL@CuO1**. Furthermore, a linear correlation was observed between cathodic peak current versus square root of scan as shown in figure SF2. The slope of the linear curve is used to calculate the diffusion control of Cu^{2+}/ Cu by applying Randles–Sevcik equation [45]

$$I_{cp} = 0.4463nFAc(\alpha nFDv/RT)^{1/2}$$

Here, $I_{cp,}$ A, D, C, R, T, α, n, and, F represents cathodic peak current, electrode area, diffusion coefficient, concentration of **ZIL@CuO1**, gas constant, absolute temperature, transfer coefficient, electron transfer number and faraday coefficient respectively. Further, to calculate the value of αn the following equation can be used.[45]

$$|E_{cp} - E_{cp/2}| = 1.857RT/\alpha nF$$

Similarly, The cathodic peak potential of **ZIL@CuO2** and **ZIL@CuO3** shown at -0.507 mV and –0.637 mV corresponding to Cu^{2+}/ Cu and the anodic peak potential shown at – 0.476, 0.457 mV. Furthermore, in the similar manner quassi-reversible nature in case of **ZIL@CuO2&3** was also observed using scan rate experiment.[46] Finally, the diffusion coefficient was calculated and in case of **ZIL@CuO1** it was found to be 1.38 x 10^{-7}. The diffusion coefficient for **ZIL@CuO2** and **ZIL@CuO3** was found to be 3.32 x10^{-7} and 9 x 10^{-7} respectively. Further, the redox behaviour of **ZIL@CuO1-3** were compared with the bare CuO as well free ionic liquid (Figure 5) and the redox data were summarized in table ST6. The experimental data clearly confirmed that the peak current density was high in case of **ZIL@CuO1-3** compared to bare copper oxide as well as ionic liquid which is due to the high porosity associated with these materials.[47] The porous nature enhances the surface reactivity andcatalytic efficiency of the catalyst which was later confirmed from their application part.

View Article Online
DOI: 10.1039/C6NJ03763A

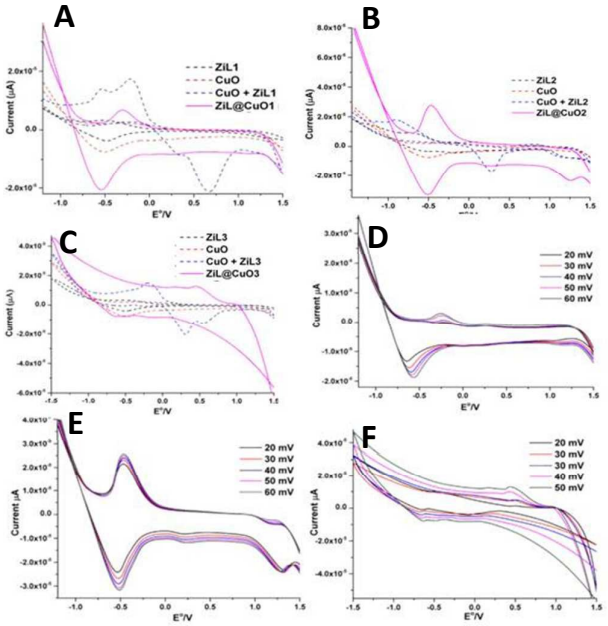

Figure 5. **(A-C),** comparative CV profile of ZILs, CuO, ZIL-Cu complex and ZIL@CuO for ZIL1, 2 and 3 respectively;**(D-F),** scan rate data for ZIL@CuO1, 2 and 3 receptively with increasing scan rate.

Surface coated ZIL quantification: The thermal stability and composition of the **ZIL@CuO1-3** were further investigated using TGA analysis (Figure. 6).

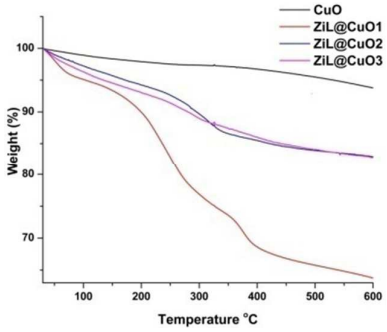

Figure 6. TGA graph of CuO and **ZIL@CuO1-3** engineered during study

Initial weight loss in case of CuO and **ZIL@CuO1-3**, it was showing from 50 to 150 °C, was due to the loss of water or some organic solvent. Thereafter, no considerable weight loss was observed for bare CuO; however, weight loss in case of **ZIL@CuO1-3** was observed and indicating the decomposition of coated **ZILs**. Here,**ZIL@CuO1**, showed about 26%, **ZIL@CuO2** showed 13% and **ZIL@CuO3** showed 12% weight loss, which represents the fraction of **ZIL**s coated on CuO nanoparticles. [48] Thus, higher fraction of **ZIL1** coating was established for **CuO@ZIL1** compared to **CuO@ZIL2-3.** Finally, on the basis of structure aspect of **ZILs** as well as experimental evidences, models of **ZIL@CuO1-3** were proposed (Figure 7). Accordingly, in case of **ZIL@CuO1** meshwork like supramolecular assembly with significantly higher size and surface area was produced (A). In case of **CuO@ZIL2-3** simpler assemblies were constructed (B and C respectively). Further, **ZIL@CuO1-3** was calcined at 500 °C for 5h and PXRD were taken again (Figure SF3). The PXRD pattern obtained showed typical peaks of CuO in all the cases. Thus, difference created in PXRD of **ZIL@CuO1-3** was due to surface coating which was burned away upon calcination.

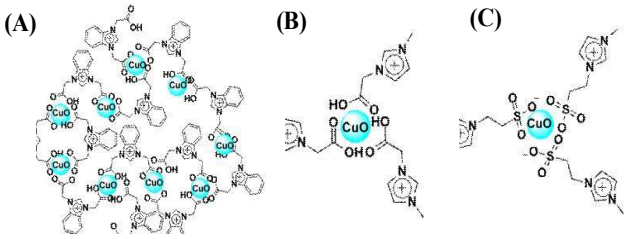

Figure 7. Structural feature of ZIL@CuO1 **(A)**, ZIL@CuO2 **(B)** and ZIL@CuO3 **(C)** catalysts produced in our study

Surface properties and acidic strength of CuO and ZIL@CuO1-3: Furthermore, to analyze the surface behaviour of CuO and **ZIL@CuO1-3**, BET studies were performed. The surface area (SA), pore volume (PV) and average pore diameter (APD) is represented in Table 1. Compared to CuO, SA, PV and APD were found to be increased in case of ZIL@CuO1-3. Herein, **ZIL@CuO1** have shown extensive increase in SA, PV and APD based parameters. N_2 adsorption isotherm of CuO and **ZIL@CuO1-3** is also represented in Figure 8. In case of **ZIL@CuO1**, the isotherm was also distinctively changed compared to CuO and **ZIL@CuO2-3.**

Table1.N_2 adsorbed BET measurements of CuO and ZIL@CuO

Sr No.	Catalyst	Surface Area m^2/g	Pore Volume cc/g	Average Pore Diameter (nm)
1	CuO	8.5	0.035	3.3
2	ZIL@CuO1	28.4	0.086	4.291
3	ZIL@CuO2	18	0.038	4.243
4	ZIL@CuO3	12	0.047	3.7

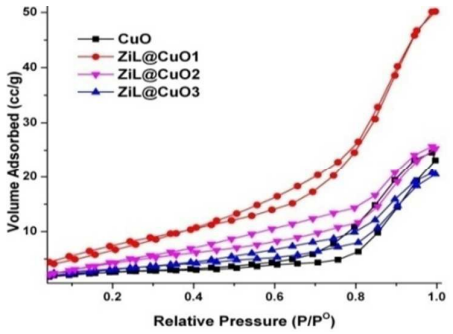

Figure8. N_2 adsorption isotherm of CuO and ZIL@CuO1-3

View Article Online
DOI: 10.1039/C6NJ03763A

Finally, the acidic strength of CuO and **ZIL@CuO1-3** were calculated, using titrametric analysis.[49] Herein 10 mg of CuO and **ZIL@CuO1-3**, were dissolved separatelyin 10 ml of 0.5N, HCl solution and stirred for half an hour. CuO NPs tends to neutralize the HCl, whereas remaining portion of HCl was estimated *via* back titrated using 0.5N sodium hydroxide solution. The results obtained are as represented in Table 2.Herein maximum basic strength per unit area was observed in case of **ZIL@CuO1** followed by **ZiL@CuO2-**3. Whereas bare CuO have shown least basic strength per unit area.

Table 2. Acidic strength calculation for CuO and ZIL@CuO

Sr. No	Catalyst	0.5N HCl Volume#	Basic unit count (BU) (mmol)##	(RBA) mmol*	Relative Basic units (RBA/1.95)**
1	**CuO**	**0.65**	1.95	1.95	1
2	**ZIL@CuO1**	**0.45**	1.4	4.67	2.4
3	**ZIL@CuO2**	**0.54**	1.62	3.43	1.75
4	**ZIL@CuO3**	**0.57**	1.71	2.41	1.23

Volume of 0.5N HCl require to neutralize 1 mg catalysts (ml)Calculated *via* Back Titration, ## Number of units equivalent to "OH" present in 1 mg of sample, *Relative surface area based exposure of basic units to reactants, calculated using formula BU X Surface area of catalyst/Surface area of CuO (Surface areas from table), ** Calculated using formula RBU X RBU/RBU for CuO

Investigation/optimization of catalytic behaviour of ZIL@CuO1-3: The reaction between 4-hydroxycoumarin and 4-hydroxybenzaldehyde was selected as a model reaction (Figure 9).

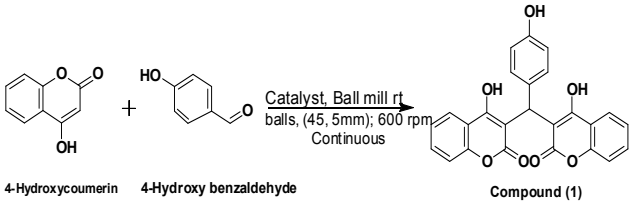

Figure 9. Reaction scheme utilized to validatethe reaction condition

In this typical reaction, 2 equivalent of 4-hydroxycoumarin, 1 equivalent of 4-hydroxybenzaldehyde and 0.5 mole% of catalyst were taken in tungsten carbide ball mill without any solvent and allowed to grind upto 240 minutes at the speed of 600 rpm. In order to optimize the reaction at different intervals of time; ^{1}H NMR of crude reaction mixture was obtained to analyze the efficacy of all combination of catalysts. The results obtained with variation in catalyst for the reaction at the end of 180 minutes is summarized in Table 3. The results clearly indicated that **ZIL@CuO1-3** significantly increased the rate of the reaction compared to parent **ZIL** or CuO with highest yield of 92% as observed for **ZIL@CuO1**. In case of **ZIL@CuO1-3** surface area, pore volume and average pore diameterwere significantly higher compared toCuO. The result signifies the role of structural parameters of engineered catalysts in determining the yield of the reaction. Thus, it is not only the **ZIL** based coator core CuO material; however the structural feature of catalysts as a whole is also critical in determining the rate of the reaction. The, highest yield obtained for **ZIL@CuO1** is attributed to the exceedingly efficient morphological aspect (Figure 3; A) as well as maximum surface area, porosity and pore diameter of **ZIL1**in case of **ZIL@CuO1** (Table 1).

Table 3. Yield at the end of 180 min of milling using different forms

Sr. No	Catalyst Specification	Catalyst Code	Yield %[a]
1	—	No Catalyst	**50**
2	Copper Oxide	CuO	**69**
3	1,3-bis(carboxymethyl)-1H-benzo[d]imidazol-3-ium bromide	ZIL1	**72**
4	3-(carboxymethyl)-1-methyl-1H-imidazol-3-ium	ZIL2	**68**
5	(1-methyl-1H-imidazol-3-ium-3-yl)methanesulfonate	ZIL3	**64**
6	1,3-bis(carboxymethyl)-1H-benzo[d]imidazol-3-ium bromide Coated on CuO-NPs	ZIL@CuO1	**92**
7	3-(carboxymethyl)-1-methyl-1H-imidazol-3-ium coated on CuO-NPs	ZIL@CuO2	**81**
8	(1-methyl-1H-imidazol-3-ium-3-yl)methanesulfonate coated CuO-NPs	ZIL@CuO3	**80**

a. Yield calculation was based on integration of ^{1}H NMR signals**.**

Further time dependent ^{1}H NMR spectrum for the reaction between 4-hydroxycoumarin and 4-hydroxybenzaldehyde was taken at different interval of time (Figure 10).At 0 min of time, typical reactant specific signals were observed; then gradual elimination of reactant specific signals at 5.5 and 9.6 clearly indicated that reactants were steadily consumed during the reaction process.

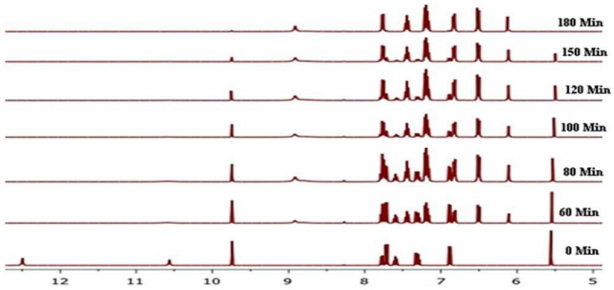

Figure 10. Time dependent ^{1}H NMR spectrum for the reaction between 4-hydroxycoumarin and 4-hydroxybenzaldehyde at different interval of time

View Article Online
DOI: 10.1039/C6NJ03763A

Similarly, the appearance of product specific signals at 6.1 indicated the product formation during the milling condition. At the end of 180 minutes the reactant specific peaks were almost eliminated and further milling produced least effects on the NMR spectrum profile of the same.

Other reaction conditions including milling speed, ball to powder ratio and reactant load were also validated to optimize the reaction scheme. To optimize the parameters, we have used ^{1}H NMR studies of reaction mixture at different time interval and monitored the progress of the reaction (Table ST7). The results obtained clearly indicated that with the increase in milling time there was continuous increase in yield up to certain edge. The, milling time of 180 min and speed of 600 rpm was found to be optimum. Furthermore, at a constant milling time of 180 min, change in milling speed also tends to influence the rate of the reaction. Increase or decrease in milling speed from 600 rpmdecreased the yield of reaction. The aforementioned observations were obvious because catalytic activity depends upon adsorption phenomenon. Thus, increase in milling speed in one hand tends to intensify the heat productions required to fulfill the activation energy need of the reaction resulted in increased yield. On the other hand continuous increase in milling speed produced excessive vibrations as well as heat thus, facilitating surface desorption of reactants from catalyst and resulted in decrease catalytic efficacy. Further, to evaluate the actual link between reaction time and heat produced, a reaction was carried out in a typical jar having special lid and a transmitter. Temperature was monitored using EASY-GTM software (Table ST8). Experiment was carried out for about one hour and results specified that temperature produced during milling condition is proportional to the milling time of the reaction.[50]According to the literature based evidences,the temperature produced inside the jar during milling is unevenly distributedwhereas, because of the mixing process, material inside the milling jar get exposed to different temperature range. [50]Herein, average temperature range exposed by reactant molecules at milling time of 180 min and milling speed of 600 rpm was found to be optimum whereas adsorption as well as activation energy needs are sufficiently satisfied and thus, producing maximum yield.The number of balls used is also an important parameter as with the increase in its number, collision frequency increases and resulted inheat production. Experiment was carried out with increasing number of balls and taking other parameters constant and 45 balls (5mm size)produced maximum yield (Table ST9).Furthermore, to investigate the ball to powder ratio, the reaction was performed using varied amount of reactant molecules and yield was found to be almost unaffected up to 1 mmol-20mmol of reactant range.Finally,proportion of 4-hydroxycoumerin and 4-hydroxy benzaldehyde was also adjusted to 2.5:1, whereas the efficacy of the catalyst was found to be unaffected but atom economy gets compromised.

Thus, considering the influence oftemperature inside the jar, and its correlation with milling time, ball number, milling speed[51] as well as^{1}HNMR based evidences, potential impact of temperature on yield of the reaction was justified and the catalytic cycle of **ZIL@CuO1-3** was further purposed (Figure 11)

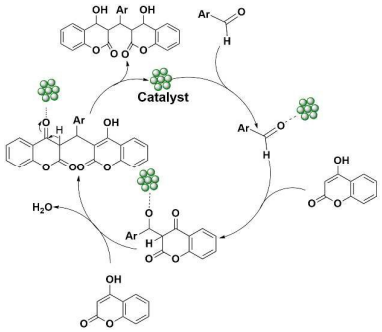

Figure 11. Plausible catalytic mechanism of ZIL@CuO1-3for the reaction

The catalytic cycle of **ZIL@CuO** initially include adsorption of reactant molecules on the surface of **ZIL@CuO.** When reactants get adsorbed on the surface of the catalyst, favorable orientation was provided and catalytic cycle was initiated (Figure 11). Initial, nucleophilic attack of 4-hydroxycoumarin occurred on the aldehydes. Here, in this step **ZIL@CuO1** activates aldehydes resulted in enhanced rate of the reaction.[52] Finally second attack of 4-hydroxycoumarin resulted in formation of bis-coumarin with regeneration of catalyst. Here coated **ZILs** as well as associated CuO both have the ability to catalyze the reaction, thus synergistic effect is observed. Finally, using aforementioned optimized conditions various other bis-coumarin analogs have also been synthesized (Figure 12). To purify the product the reaction mixture was washed with water several times. Finally, it was suspended in 10 ml of methanol to separate the products. The yield obtained was found to be more than 90% in all the cases (Figure 12). The involvement of green solvents is also a distinguishable factor, creating its real utility towards industrial scale up-gradation.

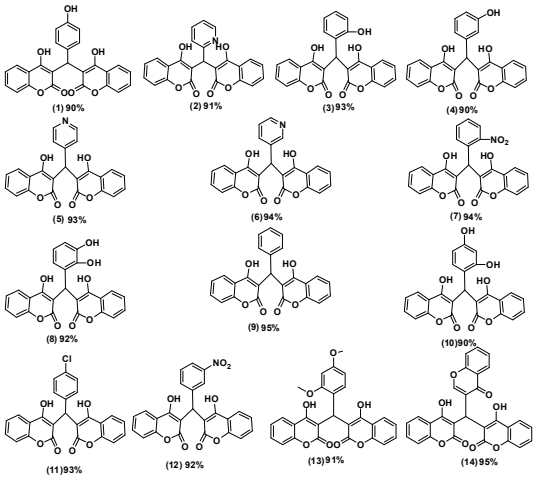

Figure 12. Structure along with yields of compounds synthesized using ball milling based strategy

View Article Online
DOI: 10.1039/C6NJ03763A

The maximum catalytic efficiency was observed for ZIL@CuO1 followed by ZIL@CuO2-3 and least for CuO. Herein, Both ZIL and CuO have the tendency to catalyze the reaction in some extend and thus hybrid of both the components, resulted in synergistic effect causing increased reaction rate in case of ZIL@CuO1-3 compared to bare CuO. Furthermore, as observed in case of BET analysis, SA, PV and APD is increased in case of **ZIL@CuO1-3** as compared to CuO. Moreover, relative basic units (Units equivalent of "OH" of base) were also increased for ZIL@CuO1-3. Thus also along with high surface area provided by ZIL@CuO1-3 compared to CuO other parameters were also favourably modified in case of ZIL@CuO1-3 resulting in increased yield. Herein, ZIL@CuO1 provided maximum SA, PV, AVD and relative basic units and thus yield obtained was also maximum.

Single crystal XRD pattern of one of the synthesized compound i.e. 3,3'-((3-nitrophenyl)methylene)bis(4-hydroxy-2H-chromen-2-one), **(12)** was solved for the purpose of characterization. It crystallizes in triclinic crystal system with space group P-1 and consists of two molecules. The ORTEP diagram along with atom numbering scheme of complex is shown in Figure 13.

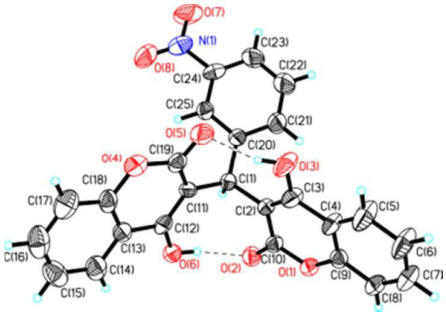

Figure 13. ORTEP diagram along with atom numbering scheme of 3,3'-((3-nitrophenyl)methylene)bis(4-hydroxy-2H-chromen-2-one), **(12)**with 40% probability thermal ellipsoids

The selected bond lengths and bond angles are given in Table ST10. In the crystal lattice, different moieties are interacting with each other through O-H…O and C-H...O hydrogen bonding interactions (Figure SF4). The hydrogen bonding parameters are given in Table ST11. Finally, characterization of all the compounds was done using ^{1}H and ^{13}C as well as elemental analysis.

The recovery and reusability of catalyst is one of the major factors to determine the cost effectiveness of the developed method. After the completion of the reaction, the reaction mixture was washed with water and finally suspended in 10 ml of methanol to precipitate the product. Finally, remaining water and methanol fraction was centrifuged at 8000 RPM for 5 min. The solid fraction so obtained was washed using 10 ml of methanol and finally with 10 ml of methanol-acetone mixture (1:1, v/v) to recover the catalyst. Recovered catalyst was further used for the reaction. The catalytic efficiency of **ZIL@CuO1** was checked up to tenth cycle of reactionwhich remained unaffected. SEM and DLS investigation of recovered catalyst after fifth (A and B) and tenth run (C and D) of the reaction is shown in Figure 14**.**

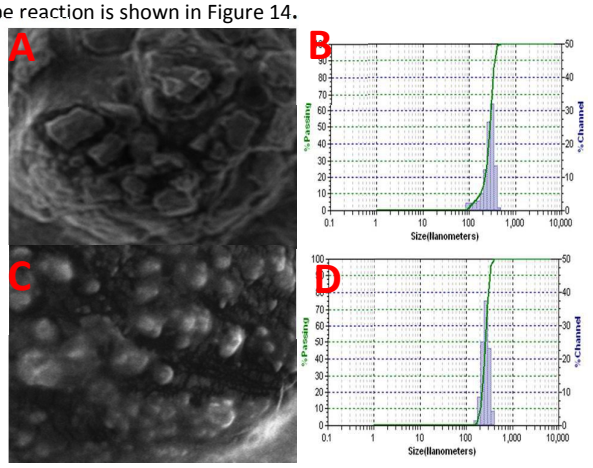

Figure 14. (A-B), SEM and DLS images of **ZIL@CuO**1 after fifth cycle and **(C-D)**,SEM and DLS images of **ZIL@CuO**1 after fifth cycle

The obtained SEM images clearly revealed that the surface texture of **ZIL@CuO**1 was significantly changed after fifth (A) and tenth (C) cycle of the reaction. Furthermore, in case of DLS study, average size of catalyst was found to be 380 nm after fifth cycle (B) and at the end of tenth cycle average size was reduced andbecame 290 nm. Herein, notable reduced size and thus significantly increased surface area as well as formation of entirely new surface morphology was observed, that was also found to be equally efficient and thus producing significant yield as observed up to tenth cycle of the reaction.

Conclusion

We have validated simple and efficient solvent free protocol for the synthesis of bis-coumarin derivatives using **ZIL** coated CuO NPs as a catalyst using ball milling technique. The advantages provided include high yield, recyclable catalyst as well as easy workup method. Furthermore, industrial scale upgradability is the major advantage provided by it over conventional methods. Green chemistry aspect is also covered with the used of least solvent during purification of product. Water and methanol which are the only solvents used belongs to the preferable category of green solvent. Thus, we have developed method which is environment friendly, and is applicable for laboratory as well as industrial scale application.

Experimental section

Materials: The starting materials were procured from various suppliers. Benzimidazole, bromoacetic acid, 1-methyl imidazole and bromo-sulfonic acid used for the synthesis of **ZILs** were obtained from Sigma Aldrich. Cuppric nitrate and sodium hydroxide used for the development of NPs were obtained from LobaChem and SDFCL respectively. Major reactants including 4-Hydroxycoumarin and benzaldehyde derivatives were again procured from Sigma Aldrich.

View Article Online
DOI: 10.1039/C6NJ03763A

Synthesis and characterization of Ionic liquids: ZILs were synthesized using chemical reaction. For the synthesis of **ZIL1,** benzimidazole (1 eq) andbromoacetic acid (2 eq) were dissolved in acetonitrile. The pH was adjusted to 8 using sodium hydroxide and refluxed for 6 h. After the completion of reaction pH was adjusted to about 2-3 to separate product. Synthesis of **ZIL2**was done by refluxing 1-methyl imidazole (1 eq) and bromo acetic acid (1 eq) at 80 ^{o}C using acetonitrile as a solvent. **ZIL3** was done using method similar to **ZIL2** by using bromo-sulfonic acid instead of bromoacetic acid. The synthesized **ZIL**s were characterized using ^{1}H, ^{13}C NMR spectroscopy (Figure SF5-7) and elemental analysis method.

Catalyst development and characterization: CuO nanoparticles were prepared using method reported in literature [53]. Initially, copper nitrate was dissolved in 100 ml of double distilled water to form 0.1 M solution. The **ZILs** were than incorporated to the aforementioned solution. The resulting solution was stirred vigorously for fifteen minutes. Finally, 0.1 M solution of NaOH was added dropwise to the vigorously stirred solution and refluxed for 2 h. The nanoparticles formed were characterized by SEM, TEM, EDX, CV and DLS based methods. The precipitates obtained were filtered washed and dried at 80 ^{o}C under vacuum condition. The dried precipitates were further characterized using PXRD, solid state UV and fluorescence spectroscopic methods.

Synthesis and characterization of bis-coumarin derivatives: Grinding beaker of 80ml with 45 balls(5 mm) were used to perform the synthesis of bis-coumarin. The grinding beakers as well as balls were made up of tungsten carbide. A concoction of 2 equivalents of 4-hydroxycoumerin, 1 equivalent of benzaldehyde derivatives and 0.5 mol% catalyst were taken in grinding beaker and milling was performed continuously for 180 min at the speed of 600 rpm. Finally, crude reaction mixture was washed with water and suspended 10 ml of methanol to get pure product. NMR technique (Table ST 12 &Figure SF 8-21) and elemental analysis was used to characterize the product.

Acknowledgement:
Mayank is thankful to IIT Ropar for fellowship

References

1. A. Viegas, J. O. Manso, M. C. Corvo, M. M. B. Marques and E. J. Cabrita, *J. Med. Chem.*, 2011, **54**, 8555-8562.
2. A. Abbott, *Nature*, 2006, **442**, 742-743.
3. A. Luqman, V. L. Blair, R. Brammananth, P. K. Crellin, R. L. Coppel and P. C. Andrews, *Eur. J Inorg. Chem.*, 2015, **2015**, 4935-4945.
4. A. G. Habeeb, P. Praveen Rao and E. E. Knaus, *J. Med. Che.*, 2001, **44**, 3039-3042.
5. K. Davies and M. Delsignore, *J. Biol. Chem.*, 1987, **262**, 9908-9913.
6. L. Benhamou, E. Chardon, G. Lavigne, S. Bellemin-Laponnaz and V. César, *Chem. Rev*, 2011, **111**, 2705-2733.
7. V. Polshettiwar and R. S. Varma, *Chem.Soc Rev.*, 2008, **37**, 1546-1557.
8. R. C. Cioc, E. Ruijter and R. V. Orru, *Green Chem*, 2014, **16**, 2958-2975.
9. K. Satyanarayana, M. R. Chandra, P. A. Ramaiah, Y. Murty, E. Pandit and S. Pammi, *Inorg. Chem. Front.*, 2014, **1**, 306-310.
10. K. C. Fylaktakidou, D. R. Gautam, D. J. Hadjipavlou-Litina, C. A. Kontogiorgis, K. E. Litinas and D. N. Nicolaides, *J. Chem. Soc., Perkin Trans. 1*, 2001, 3073-3079.
11. Z. Debeljak, A. Škrbo, I. Jasprica, A. Mornar, V. Plecko, M. Banjanac and M. Medic-Šaric, *J.Chem.Inf.Model.*, 2007, **47**, 918-926.
12. J. Neyts, E. D. Clercq, R. Singha, Y. H. Chang, A. R. Das, S. K. Chakraborty, S. C. Hong, S.-C. Tsay, M.-H. Hsu and J. R. Hwu, *J. Med. Chem.*, 2009, **52**, 1486-1490.
13. F. Han, W. Liu, L. Zhu, Y. Wang and C. Fang, *J. Mater. Chem. C*, 2016, **4**, 2954-2963.
14. M. Vashishtha, M. Mishra and D. O. Shah, *Green Chem.*, 2016, **5**, 1339-1354.
15. R. Thorwirth, A. Stolle, B. Ondruschka, A. Wild and U. S. Schubert, *Chem. Commun.*, 2011, **47**, 4370-4372.
16. H. Sharma, N. Singh and D. O. Jang, *Green Chem.*, 2014, **16**, 4922-4930.
17. M. Vashishtha, M. Mishra and D. O. Shah, *Green Chem.*, 2016, **18**, 1339-1354.
18. A. Stolle, T. Szuppa, S. E. Leonhardt and B. Ondruschka, *Chem. Soc. Rev*, 2011, **40**, 2317-2329.
19. A. Stolle, Ball milling towards green synthesis: applications, projects, challenges,*Royal Society of Chemistry*, 2014.
20. R. Thorwirth and A. Stolle, *Synlett*, 2011, **2011**, 2200-2202.
21. T. Raj, H. Sharma, Mayank, A. Singh, T. Aree, N. Kaur, N. Singh and D. O. Jang, *ACS Sus. Chem. Eng.*, 2017, DOI: 10.1021/acssuschemeng.6b02030.
22. F. Schneider, A. Stolle, B. Ondruschka and H. Hopf, *Org. Process Res. Dev.*, 2008, **13**, 44-48.
23. S. L. James, C. J. Adams, C. Bolm, D. Braga, P. Collier, T. Friščić, F. Grepioni, K. D. Harris, G. Hyett and W. Jones, *Chem. Soc. Rev.*, 2012, **41**, 413-447.
24. J. Peng and Y. Deng, *Tetrahedron Lett.*, 2001, **42**, 5917-5919.
25. Q. Zhang, S. Zhang and Y. Deng, *Green Chem.*, 2011, **13**, 2619-2637.
26. C. E. Song, W. H. Shim, E. J. Roh, S.-g. Lee and J. H. Choi, *Chem. Commun.*, 2001, 1122-1123.
27. S. Luo, L. Zhang, X. Mi, Y. Qiao and J.-P. Cheng, *J.Org Chem.*, 2007, **72**, 9350-9352.
28. B. Zhang and N. Yan, *Catalysts*, 2013, **3**, 543-562.
29. J. Isaad, *RSC Adv.*, 2014, **4**, 49333-49341.
30. H. Singh, J. Sindhu, J. M. Khurana, C. Sharma and K. Aneja, *Eur. J. Med. Chem.*, 2014, **77**, 145-154.
31. K. Tokarek, J. L. Hueso, P. Kuśtrowski, G. Stochel and A. Kyzioł, *Eur. J. Inorg. Chem.*, 2013, **2013**, 4940-4947.
32. R. Liu, J. Yin, W. Du, F. Gao, Y. Fan and Q. Lu, *Eur. J. Inorg. Chem.*, 2013, **2013**, 1358-1362.
33. B. Soberats, M. Yoshio, T. Ichikawa, H. Ohno and T. Kato, *J. Mater. Chem. A*, 2015, **3**, 11232-11238.
34. R. Sheldon, *Chem. Commun*, 2001, 2399-2407.
35. N. V. Plechkova and K. R. Seddon, *Chemical Society Reviews*, 2008, **37**, 123-150.
36. A. Singh, J. Singh, N. Singh and D. O. Jang, *Tetrahedron*, 2015, **71**, 6143-6147.

View Article Online
DOI: 10.1039/C6NJ03763A

37. A. Singh, A. Singh and N. Singh, *Dalton Transactions*, 2014, **43**, 16283-16288.
38. H. Sharma, N. Kaur, N. Singh and D. O. Jang, *Green Chem*, 2015, **17**, 4263-4270.
39. Q. Zhang, D. Sando and V. Nagarajan, *J. Mater. Chem. C*, 2016, **4**, 4092-4124.
40. M. Yin, C.-K. Wu, Y. Lou, C. Burda, J. T. Koberstein, Y. Zhu and S. O'Brien, *J.Am. Chem. Soc.*, 2005, **127**, 9506-9511.
41. S. Agnihotri, S. Mukherji and S. Mukherji, *RSC Adv.*, 2014, **4**, 3974-3983.
42. A. S. Lanje, S. J. Sharma, R. B. Pode and R. S. Ningthoujam, *Adv. Appl. Sci. Res*, 2010, **1**, 36-40.
43. B. Panigrahy, M. Aslam, D. S. Misra, M. Ghosh and D. Bahadur, *Adv. Funct. Mater.*, 2010, **20**, 1161-1165.
44. Y. Zhao, X. Song, Q. Song and Z. Yin, *CrystEngComm*, 2012, **14**, 6710-6719.
45. Q. Zhang and Y. Hua, *Phys. Chem. Chem. Phys.*, 2014, **16**, 27088-27095.
46. P. Raj, A. Singh, K. Kaur, T. Aree, A. Singh and N. Singh, *Inorganic chemistry*, 2016, **10**, 4874-4883.
47. H. H. H. M. A. Ibrahim, S. S. A. E. R. Mohammed and A. Amin, *Int. J. Electrochem. Sci*, 2010, **5**, 278-294.
48. D. Deng, Y. Cheng, Y. Jin, T. Qi and F. Xiao, *J. Mater. Chem.*, 2012, **22**, 23989-23995.
49. T. Alemdaroglu, *Commun. Fac.Sci. Univ. Ankara B*, 2001, **47**, 27-35.
50. R. Schmidt, H. M. Scholze and A. Stolle, *Int. J. Ind. Chem.*, 2016, **7**, 181-186.
51. T. Szuppa, A. Stolle, B. Ondruschka and W. Hopfe, *ChemSusChem*, 2010, **3**, 1181-1191.
52. J. Albadi, A. Mansournezhad and S. Salehnasab, *Res. Chem. Intermediat.*, 2015, **41**, 5713-5721.
53. H. Sharma, A. Singh, N. Kaur and N. Singh, *ACS Sus. Chem. Eng.*, 2013, **1**, 1600-1608.

View Article Online
DOI: 10.1039/C6NJ03763A

Zwitterionic Liquid (ZIL) Coated CuO as an Efficient Catalyst for the Green Syntheses of Bis-Coumarins derivatives *via* One-Pot Multi-component Reactions Using Mechanochemistry

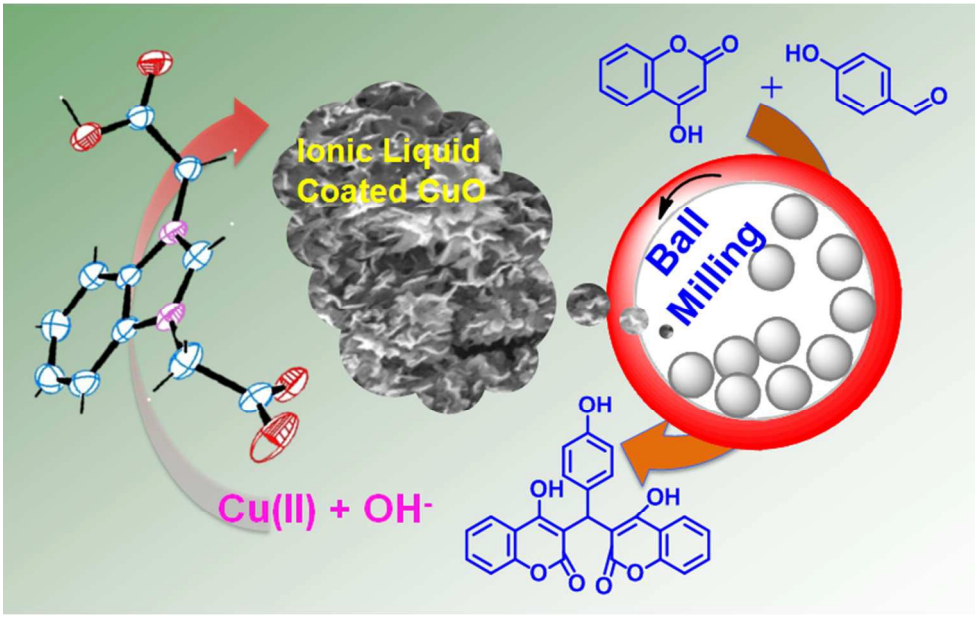

- **ZIL@CuO1-3** were developed as a catalyst for the synthesis of bis-coumarins under environmentally benign conditions.
- Mechanochemistry induced synthesis of bis-coumarin derivatives with more than 90% yield was accomplished.